Wavelength Scaling of High Harmonic Generation Close to the Multiphoton Ionization Regime

Chien-Jen Lai,[1,*] Giovanni Cirmi,[1,2] Kyung-Han Hong,[1] Jeffrey Moses,[1] Shu-Wei Huang,[1] Eduardo Granados,[1] Phillip Keathley,[1] Siddharth Bhardwaj,[1] and Franz X. Kärtner[1,2]

[1]*Department of Electrical Engineering and Computer Science and Research Laboratory of Electronics, Massachusetts Institute of Technology (MIT), Cambridge, Massachusetts 02139, USA*

[2]*Center for Free-Electron Laser Science, DESY, and Department of Physics, University of Hamburg, D-22607 Hamburg, Germany*

(Received 21 February 2013; published 12 August 2013)

We study the wavelength scaling of high harmonic generation efficiency with visible driver wavelengths in the transition between the tunneling and the multiphoton ionization regimes where the Keldysh parameter is around unity. Our experiment shows a less dramatic wavelength scaling of efficiency than the conventional case for near- and mid-IR driver wavelengths, and it is well explained by a generalized three-step model for increased Keldysh parameters that employs complex ionization times in addition to the nonadiabatic ionization. The complex ionization time is critical to avoid the divergence when replacing the quasistatic ionization model by the more general nonadiabatic ionization model. Together, the two modifications present a consistent description of the influence of the atomic potential on the rescattering process in the intermediate Keldysh regime.

DOI: 10.1103/PhysRevLett.111.073901 PACS numbers: 42.65.Re, 32.80.Rm, 42.79.Nv

High harmonic generation (HHG), a rescattering process described by the three-step model (TSM) [1,2], is an extreme nonlinear process essential to attosecond pulse generation [3–5], tabletop extreme ultraviolet (EUV) and soft x-ray sources [6–8], and HHG spectroscopy [9,10]. Driven by different wavelengths, HHG shows different cutoffs and conversion efficiencies that are important for these applications. One critical feature of HHG is the strong dependence of the single-atom efficiency (SE) on the driver wavelength λ, which scales as $\lambda^{-(5-6)}$ [11–17]. This scaling relation suggests using shorter driver wavelengths in pursuit of better conversion efficiency for lower photon energy applications [18], particularly in the EUV (<100 eV) range. In addition to the higher SE, at short driver wavelengths it is easier to maintain phase matching, and one can drive the process at a higher ionization level with higher peak intensity. These advantages further enhance the overall conversion efficiency and make HHG more of a promising mechanism for coherent EUV sources [18].

The wavelength scaling has been studied in many theoretical works [11–16] and experiments [17–24] using infrared (IR) driver wavelengths (800–2000 nm). For driver wavelengths shorter than 800 nm, the scaling has been studied by comparing the efficiencies with one near-IR driver wavelength and its second harmonic [18,22,23]. Although the second harmonic shows a dramatic enhancement of HHG efficiency, a systematic experiment employing more wavelengths is still necessary to experimentally map out the detailed wavelength scaling. To study the wavelength scaling of SE using short-wavelength drivers, the TSM needs to be applied carefully because the semiclassical picture in the conventional TSM assumes that the Keldysh parameter γ [25] is much less than one and neglects its influence. However, γ is rarely much less than one in many HHG experiments. When γ is considered, it has been shown that the ionization time at which an electron exits the atomic potential barrier is slightly advanced from the semiclassical model [26]. Since the ionization time can influence the HHG efficiency through quantum diffusion [2,27], this can lead to different HHG characteristics. To study this difference, visible driver wavelengths are more suitable than IR because γ is higher for shorter wavelengths at a given intensity.

In this Letter we study the wavelength scaling of the SE driven by visible wavelengths from a tunable optical parametric amplifier (OPA) [28] in the transition between the tunneling and the multiphoton ionization with $\gamma \approx 1$. Our experiment shows a less dramatic wavelength scaling than the conventional case with IR driver wavelengths. We show that failure of the conventional TSM to capture this trend can be repaired by generalizing the model for high-γ cases by consistent implementation of two factors: the complex saddle points of the ionization time and the nonadiabatic (NA) ionization [29]. We find that inclusion of the complex ionization time (CIT) is necessary both to capture wavelength scaling of HHG efficiency close to the multiphoton ionization regime and to prevent divergence of the TSM using the NA ionization model.

First, we clarify the definition of the HHG efficiency for wavelength scaling. A common definition is the total HHG yield within a certain range of photon energy from driver pulses that differ in the wavelengths but have the same number of electric field cycles and the same peak intensity [11–13]. With this definition, a scaling of $\lambda^{-(5-6)}$ has been reported for IR driver wavelengths [11–13]. However, this definition is not suitable for visible driver wavelengths because the HHG spectra have narrower bandwidths and

sparser harmonics. It is more appropriate to compare the single harmonic yield near some fixed photon energy with the same driver pulse energy and peak intensity [14]. To convert the former wavelength scaling relation to the latter, one should divide the former by a factor of λ^2 [30]. One λ factor is due to the higher pulse energy within the driver pulses of a fixed number of cycles and longer wavelengths [31]; the other λ factor is due to the greater number of harmonics within the fixed photon energy range for longer driver wavelengths. Here we have assumed similar efficiencies for the harmonics within the considered photon energy range, and this is usually true for the plateau harmonics. Therefore, the wavelength scaling of the SE found in previous works should be restated as $\lambda^{-(7-8)}$ for single harmonic efficiency with a fixed driver pulse energy.

The macroscopic experimental conditions have to be carefully controlled in order to extract the information of the SE without the interference from macroscopic factors [17]. The total yield of the qth harmonic can be expressed as [32]

$$S_q = C \int d\tau \int 2\pi r dr \left| \int_{-L/2}^{L/2} dz \eta \rho \exp(iz\Delta k_q) \times \exp\left[-\frac{\rho\sigma}{2}\left(\frac{L}{2} - z\right)\right]\right|^2, \quad (1)$$

where C is a proportional constant; τ is the time in the comoving frame of the driver pulse; r is the radial coordinate; z is the propagation direction; η is the SE; ρ is the medium density; L is the medium length; Δk_q is the wave-vector mismatch; and σ is the absorption cross section of the harmonic. To directly relate the measured yield S_q to the SE, we need to fix all of the parameters in Eq. (1) except η. Therefore, the driver pulses must have the same pulse duration and focal beam waist. With the same pulse energy, the peak intensity is fixed as well. We also need to make the HHG phase matched by keeping $\Delta k_q L < \pi$.

In the experiment, the driver wavelengths included three visible wavelengths from our OPA system [28] and 800 nm from the Ti:sapphire amplifier. The OPA signal was continuously tunable between 470 and 650 nm with 34–39 fs pulse duration, similar to the 35 fs pulse duration of the 800 nm pulse. We fixed the focal beam waists at 26 ± 2 μm by controlling the entrance iris before the focusing lens and measured the beam waists by the knife edge method. The similar temporal and spatial conditions of these driver pulses minimized the difference in the temporal and radial integrals in Eq. (1). The pulse energies were $\sim$90 μJ at the focus, corresponding to a peak intensity of $(2.7 \pm 0.2) \times 10^{14}$ W/cm^2. The corresponding Keldysh parameters were 0.7–1.1. The HHG medium was an Ar jet from an exit orifice with 1 mm diameter. Characterized by a Mach-Zehnder interferometer, the Ar density was 3×10^{18} cm^{-3}. The high harmonic (HH) signals were detected by an EUV spectrometer equipped with a microchannel plate.

In addition to the driver pulse conditions, another important macroscopic aspect is phase matching. Fortunately, phase matching is much easier to achieve for shorter driver wavelengths because of the lower harmonic order and the smaller Gouy phase [31]. The phase mismatch for a multicycle driver pulse may result from the neutral atom dispersion, the plasma dispersion, the Gouy phase, and the dipole phase [31–33]. With moderate peak intensities in the experiment, the neutral atom dispersion and the plasma dispersion were roughly balanced, and the residual phase mismatch was mainly due to the Gouy phase, which could be cancelled by placing the gas jet behind the laser focus to induce an appropriate amount of dipole phase [34]. To achieve phase matching, we selected the short trajectory by scanning the gas jet position and maximizing the target HH signal. To check phase matching, we measured the pressure dependence of the 21st harmonic of the 800 nm driver wavelength, which was the highest harmonic order in our experiment and therefore the most difficult one for phase matching. As shown in Fig. 1(a), when the pressure was low, the HH signal showed a quadratic dependence on the medium pressure. Thus, we ensured phase matching between the HH and the driver pulse within the interaction length.

After controlling the macroscopic parameters and optimizing the phase matching, we can directly relate the measured HH signal to the SE. We compare the 13th,

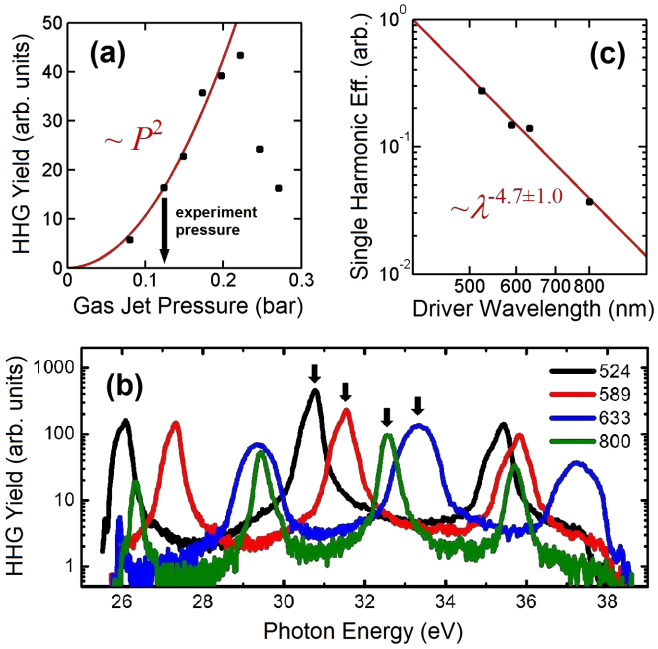

FIG. 1 (color online). (a) The pressure dependence of the 21st harmonic of the 800 nm driver pulse. The arrow indicates the pressure set in the wavelength scaling experiment for the other driver wavelengths. (b) The HHG experiment spectra, where the arrows indicate the optimized phase-matched harmonics to compare. (c) The integrated signal of the individual harmonics indicated by the arrows in (b).

15th, 17th, and 21st harmonics of the 524, 589, 633, and 800 nm driver wavelengths respectively. All of these harmonics have similar photon energy at around 32 eV, as shown in Fig. 1(b). We calculate the total HH yield within each specific harmonic peak by integrating the spectrum over the $\pm\omega_0$ neighborhood of the peak, where ω_0 is the driver frequency. The HHG efficiency of each specific harmonic peak is plotted in Fig. 1(c) and shows a wavelength scaling of $\lambda^{-(4.7\pm1.0)}$, less dramatic than the $\lambda^{-(7-8)}$ scaling observed with IR driver wavelengths. We attribute this difference to the larger Keldysh parameter and the deviation from a pure tunneling process, as will be explained by our modified TSM below.

In the conventional TSM, the HH dipole moment can be expressed as [14,15]

$$x(t_r) = \frac{(2I_p)^{1/4}}{\sqrt{i\pi}} \sum_n \frac{g(t_{b,n})g(t_r)\sqrt{w[E(t_{b,n})]}}{E(t_{b,n})[(t_r - t_{b,n})/(2\pi)]^{3/2}} a_{\mathrm{rec}} \times \exp[-iS(p, t_{b,n}, t_r)], \quad (2)$$

where I_p is the ionization potential; n denotes the trajectory; g is the ground state amplitude; w is the ionization rate that is usually calculated by the Ammosov-Delone-Krainov (ADK) formula [14,15]; E is the driver electric field; a_{rec} is the recombination amplitude; and S is the action of the electron as a function of the canonical momentum p, the ionization time $t_{b,n}$, and the recombination time t_r. To generalize Eq. (2) for higher γ, we solve the ionization time and the canonical momentum from the saddle point equations with I_p included and denote the complex solution as $\tilde{t}_{b,n}$ and $\tilde{p}$, respectively. The complex $\tilde{t}_{b,n}$ and $\tilde{p}$ are also employed in the frequency domain approach of the HH dipole moment [35]. The physical intuition behind $\mathrm{Im}(\tilde{t}_{b,n})$ is the tunneling time the electron experiences under the atomic potential barrier, and $\mathrm{Re}(\tilde{t}_{b,n})$ is the real ionization time at which the electron exits the barrier [36]. The action S is then calculated with the complex saddle point, and $\mathrm{Im}(S)$ is related to the NA ionization model w_{NA} [29] rather than the quasistatic ADK formula for a more accurate ionization rate [30,37]. The NA ionization model also takes I_p into account in the saddle point calculation of the ionization moment and shows significant corrections to the intracycle ionization of the ADK formula [29]. In addition to the modification of the action-related terms, we consistently substitute $t_{b,n}$ by $\tilde{t}_{b,n}$ and reach the following form of the modified TSM [note, $\mathrm{Im}(S)$ has been separated from the exponential term and related to the ionization formula [38], so only $\mathrm{Re}(S)$ appears explicitly],

$$x(t_r) = \frac{(2I_p)^{1/4}}{\sqrt{i\pi}} \sum_n \frac{g(\mathrm{Re}\tilde{t}_{b,n})g(t_r)\sqrt{w_{\mathrm{NA}}[E(\mathrm{Re}\tilde{t}_{b,n})]}}{E(\tilde{t}_{b,n})[(t_r - \tilde{t}_{b,n})/(2\pi)]^{3/2}} a_{\mathrm{rec}} \times \exp[-i\,\mathrm{Re}S(\tilde{p}, \tilde{t}_{b,n}, t_r)]. \quad (3)$$

With the CIT, we expect the additional time spent under the barrier to influence the wavelength scaling of the SE. To the first order approximation of γ, we can write the electron traveling time (normalized with the driver pulse phase) as [38]

$$t_r - \tilde{t}_{b,n} \approx t_r - t_{b,n} - \frac{i\gamma}{\cos(t_{b,n})}. \quad (4)$$

For a short driver wavelength, γ is large, and the imaginary part of Eq. (4) can thus change the wavelength scaling. Figure 2(a) shows the magnitude of the exact traveling time as a function of the recombination time t_r. When the driver wavelength is shorter and γ is higher, the electron has to travel for a longer cycle relative to the driver pulse before recombining with the parent atom, and therefore the traveling time is not as short as the case ignoring γ. Since the HHG efficiency favors a shorter traveling time, the increasing γ makes the wavelength scaling less dramatic when the HHG process moves from the tunneling regime to the multiphoton regime. This effect is particularly important for the short trajectories because the traveling time is more sensitive to γ with a recombination time near $\pi/2$.

We calculate the wavelength scaling of HHG SE with the modified TSM. Figure 2(b) shows the single harmonic efficiency with IR driver wavelengths ($\gamma = 0.3$–0.7), and the result is consistent with the $\lambda^{-(7-8)}$ scaling relation. With shorter driver wavelengths, Fig. 3 compares the experiment data with the conventional TSM, the modified TSM, and the time-dependent Schrödinger equation (TDSE) calculations. In the conventional TSM, the ionization time is real, and the ionization rate is calculated by the ADK formula; in the modified TSM, the CIT and the NA ionization formula are employed. In Fig. 3(b), both, short and long, trajectories of the conventional TSM show more dramatic wavelength scaling than the experimental result. In contrast, the short trajectory of the modified TSM in Fig. 3(c) agrees well with the experiment by showing a

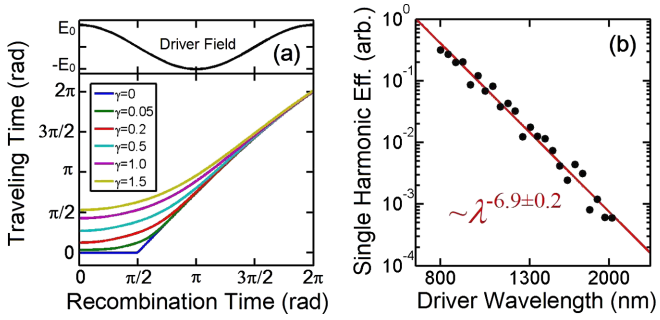

FIG. 2 (color online). (a) The magnitude of the traveling time $|t_r - \tilde{t}_{b,n}|$ as a function of the recombination time t_r for several different Keldysh parameter γ. Both of the axes are expressed in terms of the phase of the driver field. (b) The wavelength scaling of Ar SE near 32 eV calculated by Eq. (3) with IR driver wavelengths. The peak intensity of the simulated driver pulses is 2.7×10^{14} W/cm^2, and the pulse duration is 35 fs.

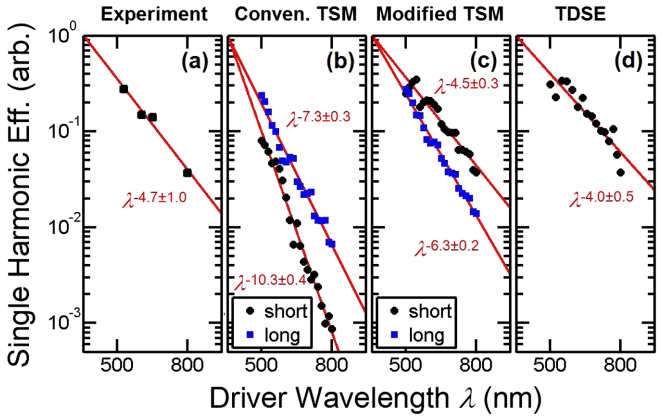

FIG. 3 (color online). Wavelength scaling of single harmonic efficiency near 32 eV (a) measured by the experiment, and calculated by (b) the conventional TSM, (c) the modified TSM, and (d) the TDSE. In (b)–(d), the peak intensity of the simulated driver pulses is 2.7×10^{14} W/cm^2, and the pulse duration is 35 fs. In the TSM calculation, the short (black dot) and long (blue square) trajectories are calculated separately, and the long trajectories are shifted by multiplying by 1.7 and 1.3 in (b) and (c), respectively, for comparison. The sums of the two trajectories scale with the driver wavelength as $\lambda^{-7.1\pm0.4}$ and $\lambda^{-4.8\pm0.3}$ in (b) and (c) (not shown), respectively.

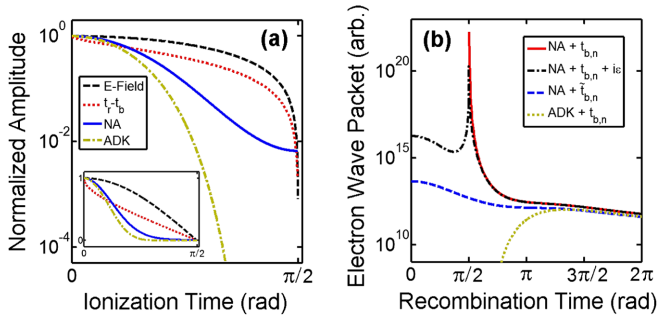

FIG. 4 (color online). (a) The comparison of the driver electric field (dashed curve), the traveling time in the conventional TSM (dotted curve), the NA ionization rate (solid curve), and the ADK ionization rate (dot-dashed curve). The horizontal axis shows the phase of the driver field, and the vertical axis shows the normalized values of the four quantities. The inlet presents the same plot on a linear scale. (b) The electron wave packet calculated with different ionization models (ADK or NA) and different ionization time formalisms ($t_{b,n}$ or $\tilde{t}_{b,n}$).

scaling of $\lambda^{-4.5}$. The long trajectory of the modified TSM has a similar scaling as the conventional TSM because the long trajectory is less sensitive to γ. The sum of the two trajectories has a scaling of $\lambda^{-4.8}$, so the short trajectories are more dominant. To further confirm this scaling relation, Fig. 3(d) shows the numerical result from the TDSE with a model potential from Ref. [39]. The wavelength scaling is $\lambda^{-4.0}$, also in good agreement with our modified TSM and experimental result.

Including the NA ionization also influences the wavelength scaling in two ways. First, the NA ionization has a higher ionization rate below the peaks of the driver field than the ADK ionization, as shown in Fig. 4(a). This enhances the short trajectory efficiency and makes it more dominant in the wavelength scaling. Second, the more uniform ionization rate close to the $\pi/2$ phase of the driver field reduces the wavelength scaling of the short trajectories. As the driver wavelength becomes longer, the efficiency of the short trajectory of some fixed photon energy decreases because the corresponding electron is ionized at a phase closer to $\pi/2$ where the field intensity is weaker [30]. The more uniform NA ionization reduces this effect on the wavelength scaling. With the CIT and the ADK ionization, a wavelength scaling of $\lambda^{-5.4}$ is obtained, and replacing the ADK by the NA ionization further improves the model and makes it closer to the experimental result.

The CIT not only improves the accuracy of the TSM, but it also avoids the divergence of the TSM due to the replacement of the ADK ionization by the NA ionization. Figure 4(a) illustrates how the divergence occurs by showing several relevant quantities. As the phase of the driver pulse at the ionization time approaches $\pi/2$, the traveling time of the conventional TSM approaches zero, while the NA ionization rate is nonzero due to the contribution from the multiphoton ionization [29], and divergence occurs. This divergence does not exist with the ADK ionization rate because the ADK rate approaches zero at a much faster rate than the traveling time. Figure 4(b) further illustrates the divergence by showing the electron wave packet that is the squared amplitude of Eq. (2) without the recombination amplitude a_{rec} [9,40]. The divergence occurs for the combination of the NA ionization and the conventional real ionization time $t_{b,n}$. When the traveling time is small, a correction factor $i\varepsilon$ in the order of I_p^{-1} may be added to the traveling time in the denominator of Eqs. (2) and (3) [2], which reflects the contribution of the atomic structure to the saddle point integrals. Unless the complex $\tilde{t}_{b,n}$ is employed, however, the electron wave packet still shows a spike even with the correction factor $i\varepsilon$, as shown in Fig. 4(b). Therefore, to apply the more general NA ionization model to the TSM, it is necessary to employ the CIT in the TSM to avoid the divergence.

In conclusion, the wavelength scaling of HHG SE is inspected experimentally and theoretically by visible driver wavelengths with a Keldysh parameter around unity in the transition between the tunneling and the multiphoton ionization regimes. The experimental result shows a less dramatic wavelength scaling than the conventional HHG with IR driver wavelengths and is well explained by our modified TSM that incorporates the NA ionization and the CIT from the saddle point method. For HHG close to the multiphoton regime, the CIT can alter the electron traveling time in the TSM and make the wavelength scaling of the SE less dramatic than HHG driven by longer wavelengths in the tunneling regime. In addition, because the

CIT removes the singularity from the traveling time in the conventional TSM, we can replace the quasistatic ADK model by the more general NA ionization model without divergence and obtain a modified TSM that works for a wider range of Keldysh parameters.

This work was supported by the Air Force Office of Scientific Research under Contract No. FA9550-12-1-0499 and the Center for Free-Electron Laser Science, DESY, Hamburg, and by Progetto Roberto Rocca. P. K. and E. G. acknowledge support by NSERC and IKERBASQUE, Basque Foundation for Science, Spain, respectively.

*cjlai@mit.edu

[1] P. B. Corkum, Phys. Rev. Lett. **71**, 1994 (1993).
[2] M. Lewenstein, Ph. Balcou, M. Yu. Ivanov, A. L'Huillier, and P. B. Corkum, Phys. Rev. A **49**, 2117 (1994).
[3] E. Goulielmakis *et al.*, Science **320**, 1614 (2008).
[4] G. Sansone *et al.*, Science **314**, 443 (2006).
[5] P. M. Paul, E. S. Toma, P. Breger, G. Mullot, F. Augé, Ph. Balcou, H. G. Muller, and P. Agostini, Science **292**, 1689 (2001).
[6] M.-C. Chen, P. Arpin, T. Popmintchev, M. Gerrity, B. Zhang, M. Seaberg, D. Popmintchev, M. M. Murnane, and H. C. Kapteyn, Phys. Rev. Lett. **105**, 173901 (2010).
[7] E. J. Takahashi, Y. Nabekawa, H. Mashiko, H. Hasegawa, A. Suda, and K. Midorikawa, IEEE J. Sel. Top. Quantum Electron. **10**, 1315 (2004).
[8] T. Popmintchev *et al.*, Science **336**, 1287 (2012).
[9] A. D. Shiner, B. E. Schmidt, C. Trallero-Herrero, H. J. Wörner, S. Patchkovskii, P. B. Corkum, J.-C. Kieffer, F. Légaré, and D. M. Villeneuve, Nat. Phys. **7**, 464 (2011).
[10] J. Itatani, J. Levesque, D. Zeidler, H. Niikura, H. Pépin, J. C. Kieffer, P. B. Corkum, and D. M. Villeneuve, Nature (London) **432**, 867 (2004).
[11] J. Tate, T. Auguste, H. G. Muller, P. Salières, P. Agostini, and L. F. DiMauro, Phys. Rev. Lett. **98**, 013901 (2007).
[12] K. Schiessl, K. L. Ishikawa, E. Persson, and J. Burgdörfer, Phys. Rev. Lett. **99**, 253903 (2007).
[13] M. V. Frolov, N. L. Manakov, T. S. Sarantseva, M. Yu. Emelin, M. Yu. Ryabikin, and A. F. Starace, Phys. Rev. Lett. **102**, 243901 (2009).
[14] E. L. Falcão-Filho, V. M. Gkortsas, A. Gordon, and F. X. Kärtner, Opt. Express **17**, 11217 (2009).
[15] V. S. Yakovlev, M. Ivanov, and F. Krausz, Opt. Express **15**, 15351 (2007).
[16] T. Auguste, F. Catoire, P. Agostini, L. F. DiMauro, C. C. Chirila, V. S. Yakovlev, and P. Salières, New J. Phys. **14**, 103014 (2012).
[17] A. D. Shiner, C. Trallero-Herrero, N. Kajumba, H.-C. Bandulet, D. Comtois, F. Légaré, M. Giguère, J.-C. Kieffer, P. B. Corkum, and D. M. Villeneuve, Phys. Rev. Lett. **103**, 073902 (2009).
[18] E. L. Falcão-Filho, C.-J. Lai, K.-H. Hong, V. M. Gkortsas, S.-W. Huang, L.-J. Chen, and F. X. Kärtner, Appl. Phys. Lett. **97**, 061107 (2010).
[19] P. Colosimo *et al.*, Nat. Phys. **4**, 386 (2008).
[20] B. Shan and Z. Chang, Phys. Rev. A **65**, 011804 (2001).
[21] E. J. Takahashi, T. Kanai, K. L. Ishikawa, Y. Nabekawa, and K. Midorikawa, Phys. Rev. Lett. **101**, 253901 (2008).
[22] T. Ditmire, J. K. Crane, H. Nguyen, L. B. DaSilva, and M. D. Perry, Phys. Rev. A **51**, R902 (1995).
[23] I. J. Kim, C. M. Kim, H. T. Kim, G. H. Lee, Y. S. Lee, J. Y. Park, D. J. Cho, and C. H. Nam, Phys. Rev. Lett. **94**, 243901 (2005).
[24] K.-H. Hong, C.-J. Lai, V.-M. Gkortsas, S.-W. Huang, J. Moses, E. Granados, S. Bhardwaj, and F. X. Kärtner, Phys. Rev. A **86**, 043412 (2012).
[25] L. V. Keldysh, Zh. Eksp. Teor. Fiz. **47**, 1945 (1964) [Sov. Phys. JETP **20**, 1307 (1965)].
[26] D. Shafir, H. Soifer, B. D. Bruner, M. Dagan, Y. Mairesse, S. Patchkovskii, M. Yu. Ivanov, O. Smirnova, and N. Dudovich, Nature (London) **485**, 343 (2012).
[27] M. Yu. Ivanov, T. Brabec, and N. Burnett, Phys. Rev. A **54**, 742 (1996).
[28] G. Cirmi, C.-J. Lai, E. Granados, S.-W. Huang, A. Sell, K.-H. Hong, J. Moses, P. Keathley, and F. X. Kärtner, J. Phys. B **45**, 205601 (2012).
[29] G. L. Yudin and M. Yu. Ivanov, Phys. Rev. A **64**, 013409 (2001).
[30] D. R. Austin and J. Biegert, Phys. Rev. A **86**, 023813 (2012).
[31] C. Jin, A.-T. Le, and C. D. Lin, Phys. Rev. A **83**, 023411 (2011).
[32] C.-J. Lai and F. X. Kärtner, Opt. Express **19**, 22377 (2011).
[33] H. Dachraoui, T. Auguste, A. Helmstedt, P. Bartz, M. Michelswirth, N. Mueller, W. Pfeiffer, P. Salieres, and U. Heinzmann, J. Phys. B **42**, 175402 (2009).
[34] P. Salières, A. L'Huillier, and M. Lewenstein, Phys. Rev. Lett. **74**, 3776 (1995).
[35] G. Sansone, C. Vozzi, S. Stagira, and M. Nisoli, Phys. Rev. A **70**, 013411 (2004).
[36] L. Torlina and O. Smirnova, Phys. Rev. A **86**, 043408 (2012).
[37] V.-M. Gkortsas, S. Bhardwaj, C.-J. Lai, K.-H. Hong, E. L. Falcão-Filho, and F. X. Kärtner, Phys. Rev. A **84**, 013427 (2011).
[38] V. M. Gkortsas, S. Bhardwaj, E. L. Falcão-Filho, K.-H. Hong, A. Gordon, and F. X. Kärtner, J. Phys. B **44**, 045601 (2011).
[39] H. G. Muller, Phys. Rev. A **60**, 1341 (1999).
[40] A.-T. Le, R. R. Lucchese, S. Tonzani, T. Morishita, and C. D. Lin, Phys. Rev. A **80**, 013401 (2009).